Available online at www.sciencedirect.com

Manufacturing Letters

Manufacturing Letters 41 (2024) 626–632

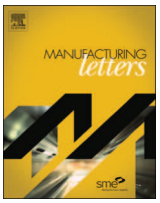

52nd SME North American Manufacturing Research Conference (NAMRC 52, 2024)

Modeling Modulated Tool Path Turning using Coupled Smoothed Particle Hydrodynamics and Finite Element method

Nishant Ojal[a,*], Ryan Copenhaver[b], Harish P Cherukuri[a], Tony L Schmitz[b], Kyle T Devlugt[c], Adam W Jaycox[c], Kyle Beith[c]

[a]*Department of Mechanical Engineering and Engineering Science, The University of North Carolina at Charlotte, Charlotte, NC 28223-0001, USA*
[b]*Department of Mechanical, Aerospace, and Biomedical Engineering, The University of Tennessee, Knoxville, TN 37996-2210, USA*
[c]*Precision Systems & Manufacturing, Lawrence Livermore National Laboratory, Livermore, CA 94550-9234, USA*

Abstract

This paper describes a full-scale, three-dimensional coupled smoothed particle hydrodynamics (SPH) and finite element model for modulated tool path (MTP) turning. The chip breaking mechanism due to modulated motion of the tool is demonstrated by the developed machining model. In contrast, the simulation of conventional turning with the same machining conditions predicts long continuous chips. The cutting force predicted by the simulation is validated with a mechanistic force model based on the instantaneous chip thickness. This work expands the capabilities of machining simulations to predict complex machining phenomena such as MTP turning through a full-scale realistic simulation. The encouraging simulation results show the potential to study more complex phenomena, such as evaluating the parameters of tool path modulation, simulating ultrasonic machining, and studying machining stability.

Keywords: Modulate tool path (MTP) machining; 3-D machining simulation; Johnson–Cook constitutive model; Smoothed particle hydrodynamics; Finite element analysis

1. Introduction

During continuous turning operations, the continuous engagement of the cutting tool with the workpiece results in long, continuous chips. These chips can affect the surface finish of the workpiece, cause tool damage and even cause an injury to the operator. Modulated tool path (MTP) turning is an effective solution to this issue. The chips are broken into smaller pieces by modulating the motion of the tool. A comparison of the chips formed by the conventional turning and MTP turning is shown in Fig. 1. In contrast to the continuous chips formed during the conventional turning, MTP turning generates broken chips. Experimental studies of MTP machining have been done for turning [1–3] and threading [4]. Copenhaver et al. [5] conducted MTP turning of tubes and compared the experimental cutting forces with analytical model results. These experimental and analytical models have been used to analyze and predict machining output [6–8]. Computational studies of machining operations have been conducted by many researchers using the Finite Element Method (FEM) [9–12]. However, there are associated challenges in modelling machining using FEM, such as high deformation, material separation and contact during machining. Due to several advantages over the grid-based approaches, smoothed particle hydrodynamics (SPH) method has garnered attention of researchers. High strains occurring in machining and chip-workpiece separation are easily modelled due to the meshless nature of the method. However, majority of the existing works are in two-dimension orthogonal machining models [13, 14] or simplified three-dimensions models [15–20]. A full-scale three-dimensional model of turning operation

* Corresponding author. Tel.: +1-704-805-0091 ; fax: +1-704-687-8345.
E-mail address: nojal@uncc.edu (Nishant Ojal).

(a) By conventional turning (b) By MTP turning

Figure 1: Comparison of chips formed by conventional and MTP turning [22].

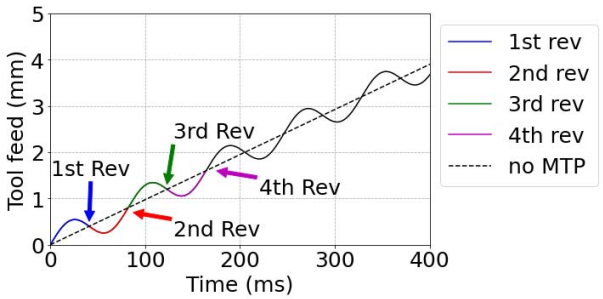

Figure 2: Tool displacement in MTP turning.

using coupled SPH-FEM approach has been presented in [21].

In this work, a coupled SPH and FEM is used to simulate the conventional and MTP turning. Chips and cutting forces predicted by these simulations are compared. Also, the results are validated using the results of a mechanistic force model based on the instantaneous chip thickness. In addition to highlighting the advantages of MTP

2. Modulated Tool Path (MTP) turning

In MTP turning, an oscillatory motion is superimposed upon the constant feed motion provided to the tool. This motion causes the tool to come out of contact with the workpiece and hence breaking the chip. Chip breakage depends upon two parameters: oscillation amplitude relative to the global feed per revolution, RAF and tool oscillation frequency relative to the spindle speed, OPR. Mathematically, these parameters are defined as

$$RAF = \frac{A}{f_r} \tag{1}$$

and

$$OPR = \frac{60f}{\omega}. \tag{2}$$

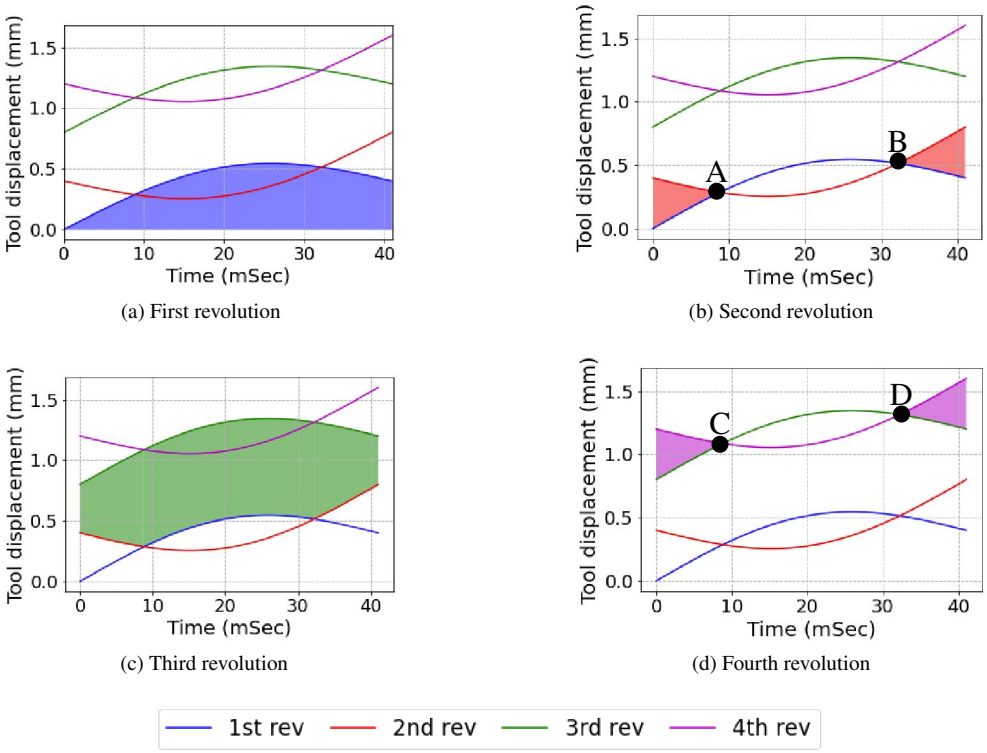

(a) First revolution (b) Second revolution

(c) Third revolution (d) Fourth revolution

Figure 3: Chip formation and breakage mechanism during MTP turning.

Here, A and f are respectively the amplitude and frequency (in Hz) of oscillation of the tool, f_r is the global feed per revolution given to the tool and ω is the spindle speed (in rpm).

An example of displacement of the tool in MTP turning is shown in Fig. 2. In this case, $RAF = 0.8$ and $OPR = 0.5$. Thus, in one cycle of the oscillation of the tool, the workpiece completes two revolutions. The black dashed line shows the displacement of the tool for conventional turning.

In MTP turning, chips break due to the oscillatory motion provided to the tool. The thickness of the chip formed in each revolution is shown in Fig. 3. This figure is obtained from Fig. 2 by fitting the tool displacement curves for each revolution in one time period of the revolution of the workpiece. In the first revolution, the area shaded by blue in Fig. 3a is machined in the form of the first chip. This chip continues in the second revolution till point A in Fig 3b. No machining occurs when the tool moves from point A to point B in the second revolution (red line), as that portion of the workpiece is already machined. The second chip starts from point B onwards and continues to grow in the third revolution, as shown by green shaded in Fig. 3c. The second chip breaks in the fourth revolution of the workpiece at point C (shown in Fig. 3d). In this way, small chips are obtained during MTP turning.

3. Computational model

A full-scale three-dimensional machining model is developed in this work using Ansys LS-DYNA® software using a coupled SPH-FE method. The SPH method is described in detail in the book by G. R. Liu and M. B. Liu [23]. In a prior work by Ojal et al.[21], the application of the SPH method to machining simulations have been discussed. SPH particles are used in the zone of cutting, where the workpiece interacts with the tool. This is a zone of high deformation. The chip forms, curls and comes in contact with itself and the surface of the tool. The FE mesh is used away from this zone, where the deformation is low. SPH particles and FE mesh are coupled at the interface. This coupling allows for the smooth transfer of the physical properties, such as displacement and stress. The coupling of SPH particles with FE mesh is accomplished by constraining the bottom layer of SPH particles with FE mesh by using the node to surface constraining algorithm. CONTACT TIED NODES TO SURFACE OFFSET keyword of LS-DYNA is used in the model. Here, the SPH elements are considered as slave part and the finite elements are considered as master part. The state variables, such as acceleration, at the interface is updated at each time step. Nodal forces and nodal mass of each slave node is distributed to the master nodes at the segment containing the contact point. Then the acceleration of the master surface is calculated. The acceleration of each slave node is then interpolated from the master segment containing its contact points (refer LS-DYNA theory manual)[24].

Renormalized SPH formulation is used in the computational model. This is because because it helps to form more realistic (curved) chip as compared to the straight chips formed by using the default formulation (Espinosa et al. [25]). Based on the study by Schwer [26], the values of "CONTROL BULK VISCOSITY" are used in the model. The value of Q1, the Quadratic viscosity coefficient, is taken as 1.5 and Q2, the Linear viscosity coefficient, is taken as 1. For the contact between SPH and solid elements, "CONTACT AUTOMATIC NODES TO SURFACE" with soft constraint penalty formulation is used. The tool is considered as master and SPH nodes are considered as slave. This formulation is recommended where the materials coming in contact have dissimilar densities and performed well during the simulation.

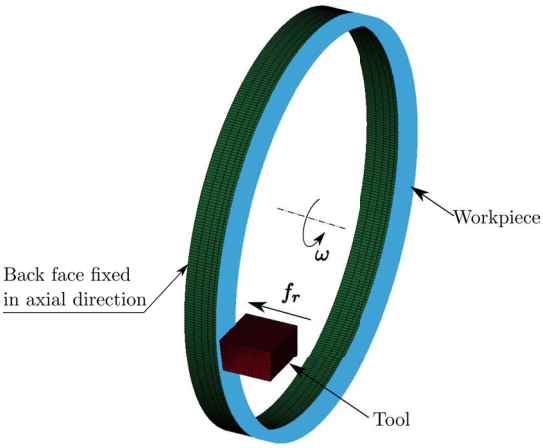

Figure 4: Computational model of MTP turning.

The coupled SPH-FE approach combines the benefits of both these methods. The challenges associated with using the FE method such as mesh distortions and material separation modelling are easily handled by the SPH method. Unlike element deletion of FE mesh in FEM to model high deformation and material separation, SPH particles move with respect to each other without any topological restrictions. This allows for the "natural" chip–workpiece separation during machining simulations. Moreover, pre-defining the separation zone at chip-workpiece separation zone in FE model for MTP turning is challenging because of the nature of tool motion. At the same time, the high computational times associated with SPH method are reduced with the use of FE mesh in the low deformation zones. Thus, coupling of SPH and FE methods results in high-fidelity and numerically efficient models. In the following, the geometry, boundary conditions and material properties used in the models are presented.

3.1. Geometry and Mesh

The computational model is shown in Fig. 4. The tool is meshed by a FE mesh and the workpiece is discretized using a coupled SPH-FE mesh. SPH particles are used in the zone of cutting, where the workpiece interacts with the tool. The FE mesh is used away from this zone, where the deformations are less. The SPH and FE mesh are coupled at the interface for the smooth transfer of physical properties. For the workpiece, SPH particles have a uniform spacing of 0.167 mm in all directions. The element size of solid element near the interface is 0.33 mm.

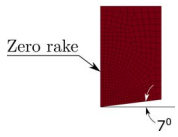

Figure 5: Geometry of the tool used.

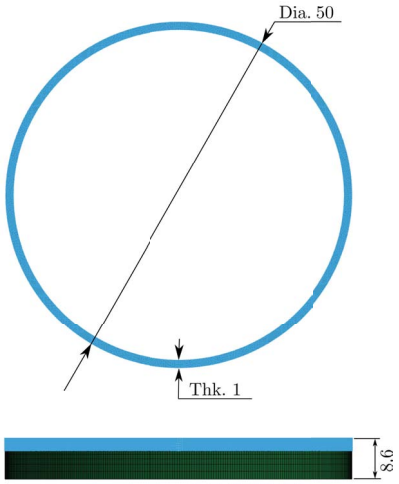

Figure 6: Geometry of the workpiece (all dimensions above are in mm).

To reduce the computation time, biased mesh along the feed direction with fine mesh at SPH-FE interface is used for the solid mesh. The maximum length of solid element in the model is 1.14 mm. In total, the workpiece consists of 78960 SPH particles and 6750 solid elements. The tool has a fine mesh with a total of 15200 solid elements. The geometry of the tool and the workpiece are shown in Fig. 5 and Fig. 6 respectively. All length dimensions are in mm. The machining conditions are provided in Table 1.

3.2. Material properties

The material of the tool is tungsten carbide and that of the workpiece is AISI 1026 steel. The physical properties of the tool and the workpiece are shown in Table 2. The tool is modeled as a rigid body. For modeling the workpiece and its fracture in the form of chips, the Johnson-Cook material model with the Johnson-Cook damage model are used. The parameters of the material model of the workpiece are shown in Table 3. The Johnson-Cook material model requires an Equation of State to be defined. *EOS LINEAR POLYNOMIAL is used with the parameter C1 set to the bulk modulus and all the other terms set to zero.

3.3. Boundary conditions

All nodes of the tool are fully constrained in Y and Z directions. A feed motion with the MTP parameters shown in Table 1 is given to the tool in X direction. All nodes of the back face of the workpiece are constrained for translation in the axial direction and a rotary motion about the axis of the workpiece is provided to them. The boundary conditions are shown in Fig. 7.

Table 1: Machining conditions used for the MTP simulation.

Parameter	**Value**
Material of tool	Tungsten carbide
Material of workpiece	1026 steel
Cutting speed	225 m/min
Global feed rate, f_r	0.4 mm/rev
RAF	0.8
OPR	0.5

Table 2: Physical properties of workpiece and tool [27, 28].

Property	Workpiece	Tool
Density, ρ (kg/m^3)	7858	11900
Young's modulus, E (GPa)	205	534
Poisson's ratio, μ	0.29	0.22
Specific heat, C_p (J/kg K^{-1})	486	-
T_{melt}, (K)	1773	-
T_{room}, (K)	300	300

Table 3: Johnson-Cook parameters of workpiece (AISI 1026 steel) [29–31].

Parameter	A (MPa)	B (MPa)	n	C	m
Value	286.1	500.1	0.2282	0.022	0.917
Parameter	D1	D2	D3	D4	D5
Value	0.403	1.107	-1.899	0.00961	0.3

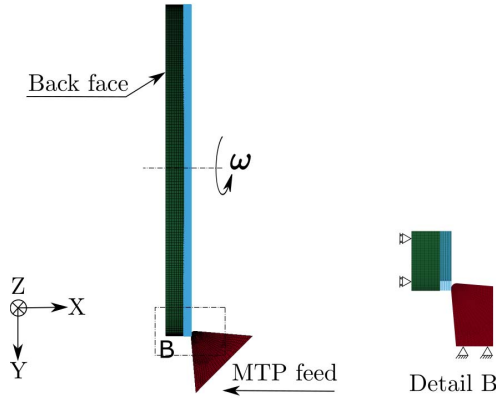

Figure 7: Boundary conditions used in MTP turning model.

3.4. Simulation time

The total simulation time for the MTP model is 157.5 hours. Two nodes of Dual 24-Core Intel Xeon Gold 6248R CPU @ 3.00GHz (48 cores per node) are used. Undoubtedly, the SPH method entails greater computational expense compared to traditional FEM. Nevertheless, in certain machining applications such as MTP machining, employing FEM poses significant

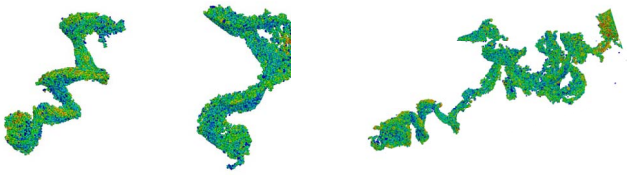

(a) MTP chips (b) Conventional turning chips

Figure 8: Chips formed by the MTP turning vs conventional turning simulation.

challenges in terms of implementation and accuracy. This is primarily due to the necessity of pre-defining zone and element deletion within FEM simulations. Creating a sinusoidal predefined zone with finite elements is challenging and requires a very fine mesh. Moreover, the process of element deletion can compromise the precision of the surface profile that the tool will encounter during subsequent rotations. To address this challenge of high computational cost, employing a combined SPH-FE model proves beneficial. Prior research [32] has illustrated the efficiency gained in computational time by utilizing the coupled SPH-FE model compared to solely employing the SPH model. As computational capabilities continue to advance, the prospect of modeling with the SPH/coupled SPH-FE model becomes increasingly promising."

4. Results

The results consist of chip profiles and cutting forces for conventional turning and MTP turning. The simulations predict long, continuous chips formed by the conventional turning and small, broken chips for the MTP turning. The comparison of chips is shown in Fig. 8. The simulated chip formation during MTP turning is shown in Fig. 9. The chip formation initiates as the tool comes into the contact with workpiece. Chip develops as the tool moves towards the workpiece. During the second revolution of the workpiece, the tool moves away from the workpiece due to the modulated feed motion given to the tool. The first chip separates when the tool is not in contact with the workpiece. Thereafter, the tool moves towards the workpiece and the second chip forms, develops and separates.

The cutting forces predicted by the simulations for the conventional and MTP turning are compared, shown in Fig. 10. For the conventional turning, a constant cutting force is observed. The cutting force for MTP turning shows a variation in the cutting force. Variation of the uncut chip thickness occurring during the MTP turning is the reason for this.

The cutting force predicted by the MTP turning simulation is compared with a mechanistic force model, described in detail in [5, 33]. In this model, the cutting force (F) is directly proportional to the chip area, A. Specific force (K_s) is the proportionality constant. The specific force depends on the variables involved in the machining operations, such as the material of

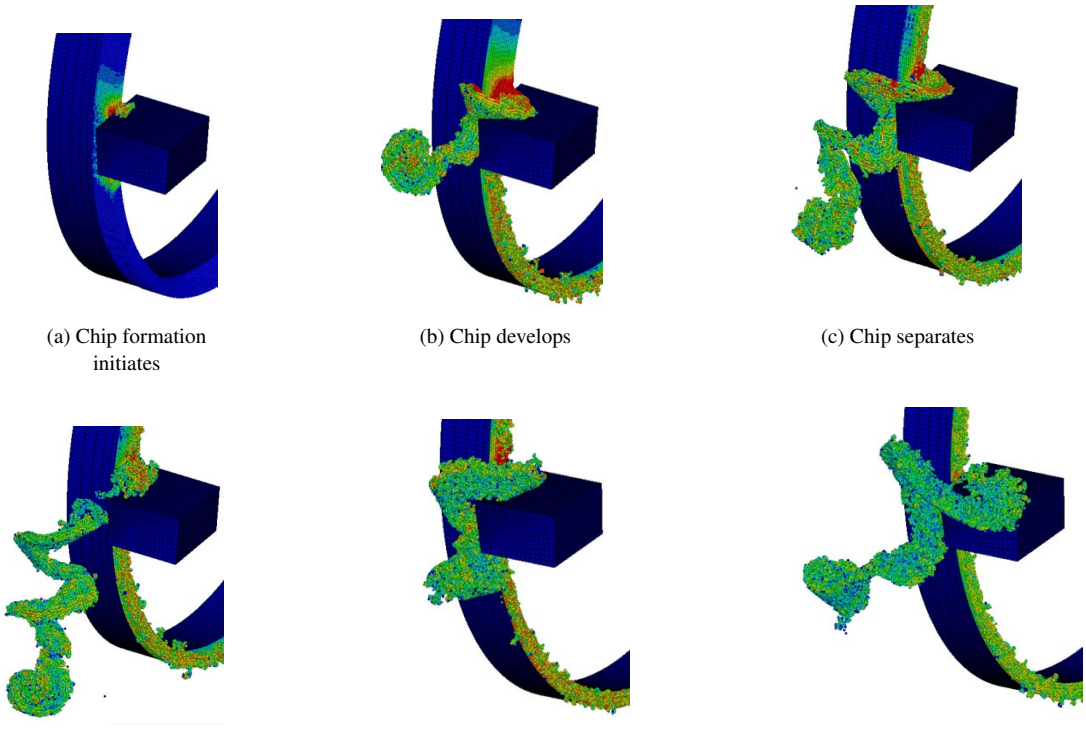

(a) Chip formation initiates (b) Chip develops (c) Chip separates

(d) 2nd chip initiates (e) 2nd chip develops (f) 2nd chip separates

Figure 9: Chip formation during MTP turning.

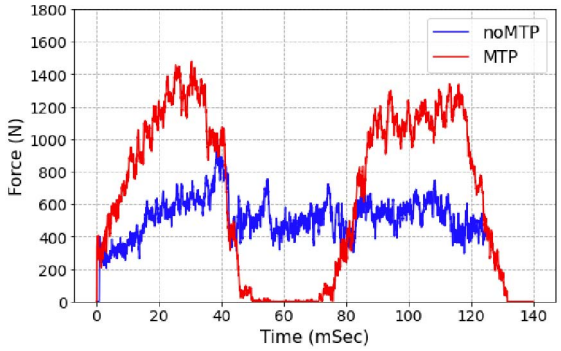

Figure 10: Cutting forces for MTP vs conventional turning simulation.

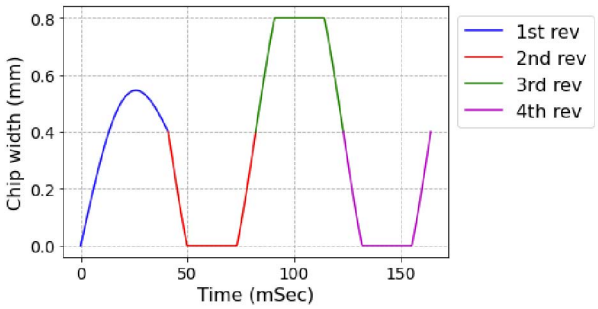

Figure 11: Instantaneous chip thickness during MTP turning.

the workpiece, tool geometry, etc. Mathematically, the cutting force is given by,

$$F = K_s A = K_s b h(t). \tag{3}$$

Here, b is the chip width, and $h(t)$ is the instantaneous chip thickness. For MTP turning, this instantaneous chip thickness is calculated by subtracting the current motion of the tool from the workpiece surface formed by the previous revolution. For the machining conditions used in the MTP turning simulation, the instantaneous chip thickness is shown in Fig 11.

The data of Copenhaver et al. [5] is used for obtaining the plot of cutting force from the analytical model. The plot of the cutting force is obtained using the value of the specific force of 1733 N/mm^2. The chip width is 1 mm. This plot is then compared with the force predicted by the simulation, as shown in Fig. 12. Good agreement between the simulated force and calculated force from the analytical model is observed.

5. Conclusions & Future work

This work incorporates the modulated tool path (MTP) in a full-scale 3D turning simulation using a coupled smoothed particle hydrodynamics and finite element method. To the best of authors knowledge, this would be the first computational model developed to study MTP turning. The results of the MTP model simulation are compared with that of the conventional

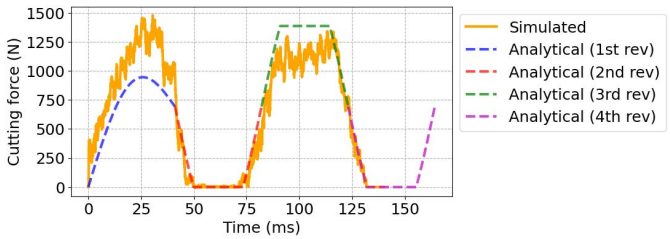

Figure 12: Comparison of simulated cutting force with the analytical model.

turning with the same machining parameters. Also, the cutting force predicted by the simulation is validated with a mechanistic force model based on the instantaneous chip thickness.

1. Different stages of chip breaking mechanism of MTP turning are simulated by the machining model. In contrast, the simulation of the conventional turning with the same machining conditions predicts long continuous chips. These results are in line with the experimental observations.
2. The cutting force predicted by the MTP turning model fluctuates with time, whereas it is continuous for the conventional turning.
3. The cutting force predicted by the MTP turning model is validated with a mechanistic force model.

Future work can include developing upon the computational model presented in this work to evaluate and improve parameters of modulated tool path turning. Other machining techniques such as vibration-assisted turning and interrupted turning can be modeled. Currently, these techniques are being studied using the experiments. Computational modeling can provide an efficient approach to optimize the parameters of these processes and improve the quality of the machined surface.

Acknowledgements

This work was performed under the auspices of the U.S. Department of Energy by Lawrence Livermore National Laboratory under Contract DE-AC52-07NA27344, LLNL-CONF-857115.

References

[1] TS Assaid. Generation, measurement, and assessment of modulated toolpath chip breaking in cnc turning processes. *Master's Thesis, UNC Charlotte, Charlotte, North Carolina*, 2010.

[2] David Andrew Tursky. *Chip Breaking Through Oscillating CNC Tool Paths and Its Effect on Chip Length, Tool Wear, and Machine Dynamics*. PhD thesis, University of North Carolina at Charlotte, 2010.

[3] Luke Berglind and John Ziegert. Chip breaking parameter selection for constant surface speed machining. In *ASME 2013 International Mechanical Engineering Congress and Exposition*. American Society of Mechanical Engineers Digital Collection, 2013.

[4] Luke Berglind and John Ziegert. Modulated tool path (MTP) machining for threading applications. *Procedia Manufacturing*, 1:546–555, 2015.

[5] Ryan Copenhaver, Mark A Rubeo, Steven Guzorek, Saurabh Landge, K Scott Smith, John Ziegert, and Tony L Schmitz. A fundamental investi-

gation of modulated tool path turning mechanics. *Procedia Manufacturing*, 10:159–170, 2017.

[6] Ryan Copenhaver, Tony Schmitz, and Scott Smith. Stability analysis of modulated tool path turning. *CIRP Annals*, 67(1):49–52, 2018.

[7] Ryan Copenhaver and Tony Schmitz. Modeling and simulation of modulated tool path (mtp) turning stability. *Manufacturing Letters*, 24:67–71, 2020.

[8] Ryan Copenhaver, Scott Smith, and Tony Schmitz. Surface prediction and measurement for modulated tool path (mtp) turning. *Manufacturing Letters*, 29:74–78, 2021.

[9] B Zhang and A Bagchi. Finite element simulation of chip formation and comparison with machining experiment. *Journal of Engineering for Industry*, 1994.

[10] Tarek Mabrouki, François Girardin, Muhammad Asad, and Jean-François Rigal. Numerical and experimental study of dry cutting for an aeronautic aluminium alloy (a2024-t351). *International Journal of Machine Tools and Manufacture*, 48(11):1187–1197, 2008.

[11] John T Carroll III and John S Strenkowski. Finite element models of orthogonal cutting with application to single point diamond turning. *International Journal of Mechanical Sciences*, 30(12):899–920, 1988.

[12] M Movahhedy, MS Gadala, and Y Altintas. Simulation of the orthogonal metal cutting process using an arbitrary lagrangian–eulerian finite-element method. *Journal of Materials Processing Technology*, 103(2):267–275, 2000.

[13] Jérôme Limido, Christine Espinosa, Michel Salaün, and Jean-Luc Lacome. SPH method applied to high speed cutting modelling. *International Journal of Mechanical Sciences*, 49(7):898–908, 2007.

[14] Yao Xi, Michael Bermingham, Gui Wang, and Matthew Dargusch. SPH/FE modeling of cutting force and chip formation during thermally assisted machining of Ti6Al4V alloy. *Computational Materials Science*, 84:188–197, 2014.

[15] I Llanos, JA Villar, I Urresti, and PJ Arrazola. Finite element modeling of oblique machining using an arbitrary lagrangian–eulerian formulation. *Machining science and technology*, 13(3):385–406, 2009.

[16] Alaa Olleak and Tugrul Özel. 3D finite element modeling based investigations of micro-textured tool designs in machining titanium alloy Ti-6Al-4V. *Procedia Manuf*, 10:536–545, 2017.

[17] Tugrul Özel, I Llanos, J Soriano, and P-J Arrazola. 3D finite element modelling of chip formation process for machining Inconel 718: comparison of FE software predictions. *Machining Science and Technology*, 15(1):21–46, 2011.

[18] Bin Shi, Ahmed Elsayed, Ahmed Damir, Helmi Attia, and Rachid M'Saoubi. A hybrid modeling approach for characterization and simulation of cryogenic machining of ti–6al–4v alloy. *Journal of Manufacturing Science and Engineering*, 141(2), 2019.

[19] Guoliang Liu, Chuanzhen Huang, Rui Su, Tugrul Özel, Yue Liu, and Longhua Xu. 3d fem simulation of the turning process of stainless steel 17-4ph with differently texturized cutting tools. *International Journal of Mechanical Sciences*, 155:417–429, 2019.

[20] Panagiotis Kyratsis, Anastasios Tzotzis, Angelos Markopoulos, and Nikolaos Tapoglou. Cad-based 3d-fe modelling of aisi-d3 turning with ceramic tooling. *Machines*, 9(1):4, 2021.

[21] Nishant Ojal, Ryan Copenhaver, Harish P Cherukuri, Tony L Schmitz, Kyle T Devlugt, and Adam W Jaycox. A realistic full-scale 3d modeling of turning using coupled smoothed particle hydrodynamics and finite element method for predicting cutting forces. *Journal of Manufacturing and Materials Processing*, 6(2):33, 2022.

[22] M Rubeo, Ryan Copenhaver, Saurabh Landge, and T Schmitz. Experimental platform for in-process metrology during orthogonal turning. In *American Society for Precision Engineering Annual Meeting, October*, pages 23–28, 2016.

[23] Gui-Rong Liu and Moubin B Liu. *Smoothed particle hydrodynamics: a meshfree particle method*. World scientific, 2003.

[24] Hallquist Jo. LS-DYNA theory manual. *LSTC, Livermore-California*, 2006.

[25] Christine Espinosa, Jean-Luc Lacome, Jérôme Limido, Michel Salaün, Catherine Mabru, and Rémy Chieragatti. Modelling high speed machining with the sph method. 2008.

[26] Leonard E Schwer and CA Windsor. Aluminum plate perforation: a comparative case study using lagrange with erosion, multi-material ale, and smooth particle hydrodynamics. In *7th European LS-DYNA conference*, volume 28, 2009.

[27] AISI 1026 Steel, cold drawn, 19-32 mm (0.75-1.25 in) round. http://www.matweb.com/search/DataSheet.aspx?MatGUID=f3c08781eced413ebd167d9a9d1211f2&ckck=1, . (Accessed on 9/16/2023).

[28] AISI 1026 Chemical Composition, AISI 1026 Mechanical Properties, AISI 1026 Heat Treatment. https://www.steelgr.com/Steel-Grades/Carbon-Steel/aisi-1026.html, . (Accessed on 9/16/2023).

[29] Shawoon Roy, Mohamed Trabia, Brendan O'Toole, Jagadeep Thota, Richard Jennings, Deepak Somasundarum, Melissa Matthes, Steven Becker, Edward Daykin, Robert Hixson, et al. Plastic deformation of steel plates under high impact loading. Technical report, Nevada Test Site/National Security Technologies, LLC (United States), 2013.

[30] JD Seidt, A Gilat, JA Klein, and JR Leach. High strain rate, high temperature constitutive and failure models for EOD impact scenarios. In *Proceedings of the SEM Annual Conference & Exposition on Experimental and Applied Mechanics*, volume 15. Society for Experimental Mechanics, 2007.

[31] ASTM A36 Carbon Steel vs. SAE-AISI 1026 Steel: Makeitfrom.com. https://www.makeitfrom.com/compare/ASTM-A36-SS400-S275-Structural-Carbon-Steel/SAE-AISI-1026-G10260-Carbon-Steel. (Accessed on 9/16/2023).

[32] Nishant Ojal, Harish P Cherukuri, Tony L Schmitz, and Adam W Jaycox. A comparison of smoothed particle hydrodynamics (sph) and coupled sph-fem methods for modeling machining. In *ASME International Mechanical Engineering Congress and Exposition*, volume 84485, page V02AT02A036. American Society of Mechanical Engineers, 2020.

[33] Tony L Schmitz and K Scott Smith. *Machining dynamics*. Springer, 2014.